Proc. Natl. Acad. Sci. USA
Vol. 81, pp. 5719–5723, September 1984
Biophysics

Theory of Mössbauer spectra of proteins fluctuating between conformational substates

(Brownian dynamics/moment expansion/protein dynamics)

WALTER NADLER AND KLAUS SCHULTEN

Physik-Department, Technische Universität München, 8046 Garching, and Max-Planck-Institut für Biophysikalische Chemie, 3400 Göttingen, Federal Republic of Germany

Communicated by Hans Frauenfelder, April 12, 1984

ABSTRACT **Mössbauer spectra of ^{57}Fe in proteins fluctuating between different conformational substates are evaluated by means of a two-sided Padée approximation, which can reproduce the low and high frequency dependence of the spectral line shape $I(\omega)$ to any desired accuracy. The dynamics of the atom is modeled as Brownian motion in a multiminimum potential and described by a Fokker–Planck equation. The Mössbauer spectrum is expanded in terms of Lorentzian contributions, which can be attributed separately to fluctuations between conformational substates (potential minima) and to relaxation within the substates. In the limit of closely spaced substates, the Mössbauer spectra can be accounted for by an effective diffusion coefficient with Arrhenius-type temperature dependence. We demonstrate that the observed temperature dependence of Mössbauer spectra of proteins [Parak, F., Knapp, E. W. & Kucheida, D. (1982) *J. Mol. Biol.* 161, 177–194] can be accounted for by stochastic motion in a multiminimum potential.**

In recent years experimental and theoretical investigations have focussed on the dynamic aspect of protein structure and function. High resolution x-ray scattering data revealed that proteins exhibit innate temperature-dependent conformational distributions (1). These distributions may be related to the functional states of proteins as indicated by rate constant measurements (2). The question arises which dynamic processes produce the observed conformational distributions. This question cannot be answered by x-ray scattering, which reveals only the static distribution of atoms. A valuable extension of these observations is provided by Mössbauer spectroscopy, which probes the motion of an excited atomic nucleus during the lifetime of its excitation.

The information entailed in a Mössbauer spectrum can best be characterized in the case of ^{57}Fe, the most common Mössbauer atom. Observation of this atom as a constituent of heme groups and iron-sulfur redox centers in proteins is of obvious interest. Mössbauer spectral data over a broad temperature range have been obtained for a number of proteins, including myoglobin (3–7), hemoglobin (8), cytochrome (9), and ferritin (10).

In an analysis of Mössbauer data, the observed spectral line shape function $I(\omega)$ is usually expanded in terms of Lorentzian lines

$$I(\omega) = (\sigma_o\Gamma/2)\mathrm{Re}\left\{\sum_{n=0}^{N-1} f_n/(\Gamma_n + i\omega)\right\}. \qquad [1]$$

The quantities appearing in this expansion will be discussed further below. The quality of the observations usually justifies only a fit of two or three Lorentzian lines. Furthermore, the accuracy of the data is significant only in the central, low frequency part of $I(\omega)$ and covers solely frequencies between 1 and $\approx$100 times the natural linewidth Γ. The linewidth of ^{57}Fe is $\Gamma = 7 \times 10^6\ s^{-1}$—i.e., the Mössbauer spectrum probes the motion of this atom for times between about 1 ns and 100 ns. On this time scale, the motion of a single atom in a protein is actually part of a concerted motion involving a larger protein fragment and, therefore, a large effective mass. One can safely consider this motion as classical, influenced by thermal noise and friction. In fact, one can expect that the motion is in the strong friction limit. By assuming the magnitude of the thermal noise to increase linearly with temperature (11), the fluctuation–dissipation theorem dictates a diffusion coefficient with a linear temperature dependence $D = D_0T$. Mössbauer spectroscopy actually observes only the Fourier component of the spatial motion that corresponds to the wavelength $\lambda = 0.86$ Å of the γ-quantum emitted by ^{57}Fe. Molecular dynamics simulations (12) show that relaxation on this length scale occurs within less than 10 ps. Accordingly, the effective diffusion coefficient D of the ^{57}Fe atom should assume values small compared to $\Gamma\lambda^2$, and only the slowest Brownian processes—e.g., barrier crossings—should contribute to the observed Mössbauer spectrum.

The discussion above suggests that a proper theory of Mössbauer line shapes must reproduce well the low-frequency part of $I(\omega)$. In addition, one wishes to describe correctly the total intensity $\int d\omega I(\omega)$. We have introduced an algorithm (13) involving a generalization of the first-passage-time approximation (14, 15), which can reproduce the total intensity and the low-frequency behavior of $I(\omega)$ to any desired accuracy. In ref. 13 the algorithm had been tested for Mössbauer spectra of Brownian particles in a harmonic potential and applied to a double-minimum potential, a case for which results were not obtainable previously. In this paper we will extend the application to realistic models of protein dynamics.

The temperature dependence of Mössbauer-spectra observed for proteins reveal with increasing temperature a sharp decrease of the Lamb–Mössbauer factor—i.e., the amplitude of the resonant line—and an accompanying broad line with increasing linewidth. It is, of course, most desirable to understand this observation in terms of the actual protein dynamics. According to the investigations of Frauenfelder *et al.* (1, 2), the dynamics of proteins involve transitions between many conformational substates. The most simple representation of these substates is furnished by a one-dimensional multiminimum potential. Hence, we will apply in this paper the algorithm of ref. 13 to Brownian motion in such potentials and study the temperature dependence of the resulting Mössbauer spectra. We also will consider the case of closely spaced substates and show that, in this limit, the substates may be accounted for by an effective diffusion coefficient with an Arrhenius-type temperature dependence. Finally, we will demonstrate that the observed temperature dependence of Mössbauer spectra (5, 16) can be accounted for by stochastic motion in a multiminimum potential.

The publication costs of this article were defrayed in part by page charge payment. This article must therefore be hereby marked "*advertisement*" in accordance with 18 U.S.C. §1734 solely to indicate this fact.

Method

We briefly summarize the algorithm introduced in ref. 13. The distribution function $p(x, t)$ of a Brownian particle with diffusion coefficient $D = D_0T$ in a potential $U(x)$ is described by the Fokker–Planck equation,

$$\partial_t p(x, t) = L(x)p(x, t), \quad [2]$$

$$L(x) = \partial_x D[\partial_x + \beta U'(x)], \quad [3]$$

together with appropriate boundary conditions that assure particle-number conservation. The solution of Eq. **2** for long times develops into the Boltzmann distribution $p_0(x) \sim \exp[-\beta U(x)]$. The Mössbauer lineshape function $I(\omega)$ can be expressed in terms of $L(x)$ by means of the following equations:

$$I(\omega) = (\sigma_0\Gamma/2)\mathrm{Re}\{\sigma(\omega)\}, \quad [4]$$

$$\sigma(\omega) = \int dx\, \exp(ikx)[i\omega - L(x) + \Gamma/2]^{-1}\exp(-ikx)p_0(x). \quad [5]$$

Spectral expansion of the structure function $\sigma(\omega)$ yields

$$\sigma(\omega) = \sum_{n=0}^{\infty} |\hat{\psi}_n(k)|^2[i\omega - \lambda_n + \Gamma/2]^{-1}. \quad [6]$$

Here $\lambda_n \leq 0$ denotes the eigenvalues of $L(x)$ assumed to be discrete, and $\hat{\psi}_n(k)$ denotes the corresponding Fourier-transformed nonorthogonal eigenfunctions with normalization $\int dx \psi_n^2(x)p_0^{-1}(x) = 1$. However, the spectral expansion (Eq. **6**) does not provide a procedure for an evaluation of Mössbauer spectra except for very simple potentials—e.g., for a square well and a harmonic (13, 17) potential.

Observed lineshape functions are usually fitted by means of Eq. **1** for a few Lorentzian lines. Accordingly, we also seek for the theoretical description of the lineshape an approximate structure function $s(\omega) \simeq \sigma(\omega)$ in terms of N Lorentzian contributions,

$$s(\omega) = \sum_{n=0}^{N-1} f_n/(i\omega + \Gamma_n). \quad [7]$$

This approximate $s(\omega)$ can be chosen to reproduce the N_h leading terms of the high-frequency expansion of $\sigma(\omega)$,

$$\sigma(\omega) \underset{\omega\to\infty}{\sim} \frac{1}{i\omega}\sum_{n=0}^{\infty} \mu_n\left(-\frac{1}{i\omega}\right)^n, \quad [8]$$

and the N_l leading terms of the low-frequency expansion,

$$\sigma(\omega) \underset{\omega\to 0}{\sim} \sum_{n=0}^{\infty} \mu_{-(n+1)}(-i\omega)^n, \quad [9]$$

where $2N = N_h + N_l$. $s(\omega)$ as defined in Eq. **7** can be viewed as the partial-fraction expansion of a $[N - 1, N]$ Padée approximant. Conditions **8** and **9** characterize then the algorithm presented here as a two-sided Padée approximation (18, 19). The appropriate amplitudes f_n and linewidths Γ_n in Eq. **7** must obey the conditions

$$\sum_{n=0}^{N-1} f_n\Gamma_n^m = \mu_m,\ m = -N_l, -N_l + 1, \ldots, N_h - 1. \quad [10]$$

This shows that for an N Lorentzian description, $2N$ conditions (Eq. **10**) have to be met. The proposed algorithm depends on a knowledge of the expansion coefficients μ_n in Eqs. **8** and **9**—the so-called *generalized moments*:

$$\mu_n = (-1)^n \int dx\, \exp(ikx)[L(x) - \Gamma/2]^n\exp(-ikx)p_0(x). \quad [11]$$

The evaluation of μ_n for positive n is straightforward. For negative n one can use a discretization scheme for the differential operator, resulting in a tridiagonal matrix for L and, thereby, evaluate the μ_n numerically (see ref. 13). Hence, the μ_n can be constructed to include any desired feature of model potential surfaces. If the spectral expansion (Eq. **6**) is known, the moments can be evaluated by means of

$$\mu_n = \sum_{m=0}^{\infty} (\Gamma/2 - \lambda_m)^n|\hat{\psi}_m(k)|^2. \quad [12]$$

In this case the algorithm gives a good description of the spectrum in terms of a few lines, whereas a truncation of Eq. **6** after the first few terms may result in a bad approximation.

We have demonstrated (13) that, in case of a double minimum potential, a three-Lorentzian description with $N_h = 1$ and $N_l = 5$ yields an accurate lineshape function. This description reproduces only the leading term of the high-frequency expansion (Eq. **8**) that carries the total intensity of $I(\omega)$. The results showed that further terms in Eq. **8** can be neglected. For Brownian dynamics in potentials with more than two minima, an accurate description of the lineshape function should involve more Lorentzian lines. Since for $N \geq 3$ the algebraic solution of Eqs. **10** is cumbersome, we determined f_n and Γ_n through an equivalent matrix representation (20).†

Results for model potentials

We assume a situation where conformational substates have identical free energies. This situation is modeled by the potential

$$U(x) = b\, \exp[-\sin^2(n\pi x/2x_0)], \quad [13]$$

where $b(e - 1)/e$ is the height of the barriers between adjacent substates. The stochastic motion of the ^{57}Fe Mössbauer atom governed by this potential will be confined to the interval $0 \leq x \leq 2x_0$. The number of substates is then n.

As an illustration for the typical temperature dependence of the Mössbauer spectrum we consider the case $n = 4$. Fig. 1 presents the linewidths and amplitudes resulting from an application of the algorithm according to Eqs. **8–12** with $N_h = 1$ and $N_l = 9$—i.e., involving five Lorentzian contributions. Each Lorentzian line describes a certain relaxation process. The linewidths in Fig. 1 *Upper* show that the relaxation processes can be grouped into four slow processes (Γ_0–Γ_3) and one fast process (Γ_4).

The fast process can be attributed to relaxation within the individual wells. This supposition is proved by the appearance of the same linewidth value for a single-well potential. In fact, one can provide approximations for the linewidth and amplitude of the fast relaxation process solely in terms of single-well properties (unpublished results):

$$\alpha_s/\gamma_s = \int_a^b dx[Dp_{0_s}(x)]^{-1}\left|\int_a^x dy\ p_{0_s}(y)[\exp(iky) - \hat{p}_{0_s}(k)]\right|^2,$$

$$\alpha_s = 1 - |\langle\exp(ikx)\rangle_s|^2. \quad [14]$$

Here α_s denotes the approximate amplitude; γ_s, the approximate linewidth; $p_{0_s}(x)$, the Boltzmann distribution inside a single wall; and $p_{0_s}(k)$, its Fourier transform. $\langle\ \rangle_s$ denotes the thermal average over a single well, and a and b stand for integration limits around a well. The α_s and γ_s determined from Eqs. **14** are in very close numerical agreement with f_4 and Γ_4 in Fig. 1. We like to point out, however, that the Fokker–Planck equation may be inadequate to describe mo-

†There is a typographical error in ref. 20, equation 20, where a should be replaced by a^N.

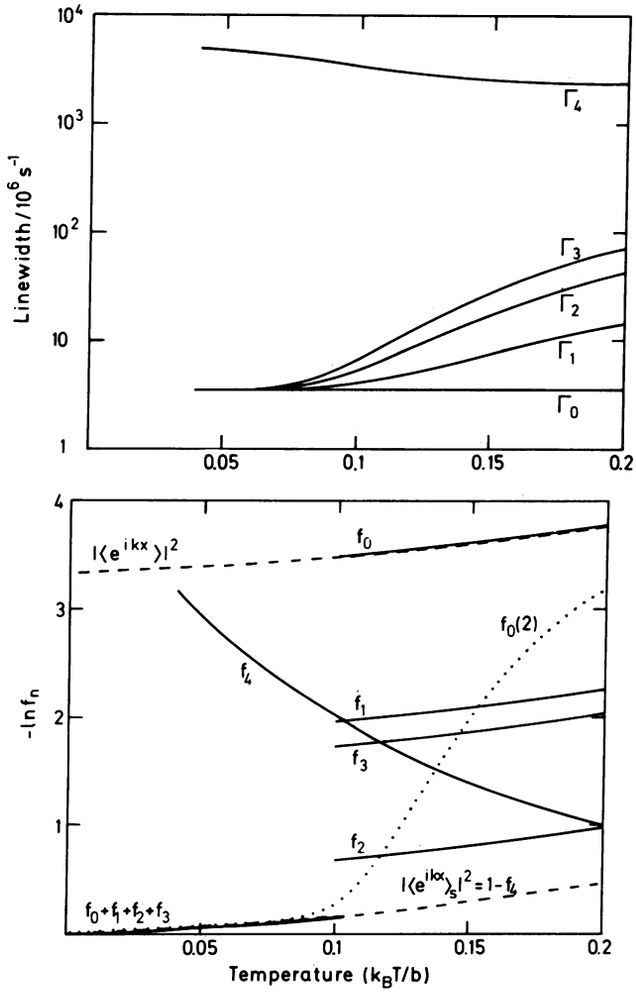

FIG. 1. Linewidths (*Upper*) and amplitudes (*Lower*) for a ^{57}Fe Brownian atom moving in the potential (Eq. **13**) with $n = 4$ in the interval $0 \leq x \leq 2x_0$ [$x_0 = 1.2$ Å, $D = 10^8$ (k_BT/b) Å^2·s^{-1}] resulting from a five Lorentzian representation reproducing the moments μ_0 to μ_{-9}; the amplitude $f_0(2)$ (*Lower*) has been obtained from a two-Lorentzian representation reproducing μ_0 to μ_{-3}.

tion in narrow potential wells with ensuing strong forces. This limitation will not affect the following conclusions except that the intrawell relaxation frequencies may assume different values than predicted by Eq. **14**. Since these frequencies are likely to be outside the accessible frequency window of Mössbauer spectra, the resulting error should be of no consequence.

The slow relaxation processes can be attributed to barrier crossing between adjacent substates. To demonstrate this interpretation, we note that a separation of time scales of fast intrawell and slow interwell processes is tantamount to a fractorization of the distribution function

$$p(x, t) = \sum_{i=1}^{n} p_i(t)p_s(x - x_i, t), \qquad [15]$$

where $p_s(y, t)$ describes motion in a single well assumed identical for all wells, $p_i(t)$ describes the distribution among wells, x_i denotes the position of the well minima, and the index i labels the different wells. The factor $p_s(y, t)$ accounts for the fast relaxation processes discussed above. The distribution $p_i(t)$ results from the rate equation

$$\partial_t p_i = \sum_j \mathbf{R}_{ij}p_j, \qquad [16]$$

where the $n \times n$ matrix $\mathbf{R}$ is

$$\mathbf{R} = \frac{1}{2\tau}\begin{pmatrix} -1 & 1 & 1 & & & & \\ 1 & -2 & 1 & \cdot & \cdot & \cdot & \cdot \\ 0 & 1 & -2 & & & & \\ & \cdot & & \cdot & & & \\ & \cdot & & & \cdot & & \\ & \cdot & & & & \cdot & \\ & \cdot & & & & -2 & 1 \\ & \cdot & & & & 1 & -1 \end{pmatrix} \qquad [17]$$

and τ is the first passage time between wells (15),

$$\tau = \int_a^b dx[Dp_{0_s}(x)]^{-1}\left|\int_a^x dy\, p_{0_s}(y)\right|^2. \qquad [18]$$

The amplitudes and linewidths connected with the slow processes can then be determined by means of the n eigenvalues κ_j and n eigenvectors v_j of $\mathbf{R}$, where we use the normalization $\sum_{i=1}^n v_{ji}^2\bar{p}_i^{-1} = 1$; $\bar{p}_i$ is the equilibrium distribution among the wells. With $g_j = |\sum_{l=1}^n \exp(ikx_l)v_{jl}|^2$, one derives for the linewidths and amplitudes

$$\begin{aligned} \gamma_j &= \Gamma/2 - \kappa_j \\ \alpha_j &= |\langle\exp(ikx)\rangle_s|^2 g_j \end{aligned} \qquad [19]$$

These quantities coincide numerically with the Γ_j and f_j for $j = 0$, 1, 2, and 3 in Fig. 1, thereby proving our interpretation of the slow relaxation processes.

The relaxation matrix $\mathbf{R}$ has always one vanishing eigenvalue $\kappa_0 = 0$. One should expect, therefore, that the natural line would always contribute to the Mössbauer spectrum with the amplitude α_0. However, for low temperatures at which the rate constant τ^{-1} is significantly smaller than $\Gamma/2$, the magnitudes of the eigenvalues of $\mathbf{R}$ are all less than $\Gamma/2$, and the slow relaxation processes cannot be resolved from the natural line. In this temperature range, the effective amplitude of the natural line, the Lamb–Mössbauer factor, is $f_0 + f_1 + f_2 + f_3 \simeq \alpha_0 + \alpha_1 + \alpha_2 + \alpha_3$ or, in general, is $\Sigma_j |\langle\exp(ikx)\rangle_s|^2 g_j$. This quantity is equal to $|\langle\exp(ikx)\rangle_s|^2$, an identity which is demonstrated in Fig. 1 *Lower*. At higher temperatures, when the rate constant τ^{-1} sufficiently exceeds $\Gamma/2$, the three lines with $\kappa_j < 0$ will be resolved from the natural line, and the Lamb–Mössbauer factor reduces to the Debye–Waller factor $f_0 \simeq \alpha_0 \simeq |\langle\exp(ikx)\rangle|^2$ as shown in Fig. 1 *Lower*. The temperature at which we declare the lines 0, 1, 2, and 3 resolved in Fig. 1 *Lower* is chosen rather arbitrarily. To conform to an experimental situation where the resolution is more gradual, we present in Fig. 1 *Lower* also the Lamb–Mössbauer factor $f_0(2)$ resulting from a two-line-fit algorithm using $N_h = 1$ and $N_l = 3$. $f_0(2)$ is shown to approach $|\langle\exp(ikx)\rangle_s|^2$ at low temperatures, and the Debye–Waller factor $|\langle\exp(ikx)\rangle|^2$ at higher temperatures.

Our description generalizes in an obvious way to an arbitrary number n of substates. In this case one expects n slow interwell relaxation processes and faster intrawell relaxation. Hence, a minimal description should include $n + 1$ lines. However, an experimental resolution of all slow processes may be impossible, and one may want to resort to a theoretical description with a smaller number of lines.

In the limit of large numbers of closely spaced substates, one can make a coarse-grained approximation—i.e., eliminate the fast intrawell relaxation and account for the slow interwell relaxation processes by an effective diffusion coefficient. As is well known, Brownian motion in an envelope potential with a superimposed periodic potential, if viewed

on a length scale greater than the unit-cell length, can be described by the effective diffusion coefficient (21),

$$D_{\text{eff}} = D/\langle \exp(\beta U)\rangle_p \langle \exp(-\beta U)\rangle_p. \quad [20]$$

Here, $\langle\ \rangle_p$ denotes the arithmetic average over one period. In the case of sufficiently high barriers between substates, as considered here, the diffusion coefficient can be approximated well by an Arrhenius temperature dependence $D_{\text{eff}} = \bar{D}\cdot\exp(-\beta E)$ for some activation energy E. For a demonstration of this coarse-grained approximation, we considered the periodic potential (Eq. **13**) superimposed over a square well and over a harmonic potential as envelopes.

Fig. 2 compares the two-line-fit Lamb–Mössbauer-factor $f_0(2)$ evaluated for the complete potential and for the square-well envelope potential with effective diffusion coefficient. The results demonstrate that for an increasing number of substates n, the two descriptions converge. Fig. 3 compares the two descriptions for a harmonic-oscillator envelope potential and the periodic potential (Eq. **13**) superimposed. The Lamb–Mössbauer factors in Fig. 3 *Upper* agree closely except for the trivial difficulty that the coarse-grained descriptions yield two contributions to the natural line at low temperatures, which cannot be resolved. The two contributions add to 1—i.e., the total amplitude of the natural lines agrees with the result for the complete potential. However, setting a resolution limit on the linewidths would be arbitrary; therefore, we have terminated the coarse-grained description below $k_BT/b = 0.08$. Fig. 3 *Lower* compares the linewidths. At higher temperatures the linewidths obtained by the two descriptions coincide. At lower temperatures the complete potential description yields the natural linewidth $\Gamma/2$ and a larger linewidth corresponding to intrawell relaxation. However, the latter carries only a very small amplitude. The coarse-grained description at low temperatures develops two linewidths close to $\Gamma/2$. Altogether this shows that the two descriptions yield very similar Mössbauer spectra except for small deviations at intermediate temperatures.

Comparison with experimental data

Fig. 4 shows a fit to the experimental data f_0, f_1, and Γ_1 of refs. 5 and 16, modeling the stochastic dynamics of ^{57}Fe by a

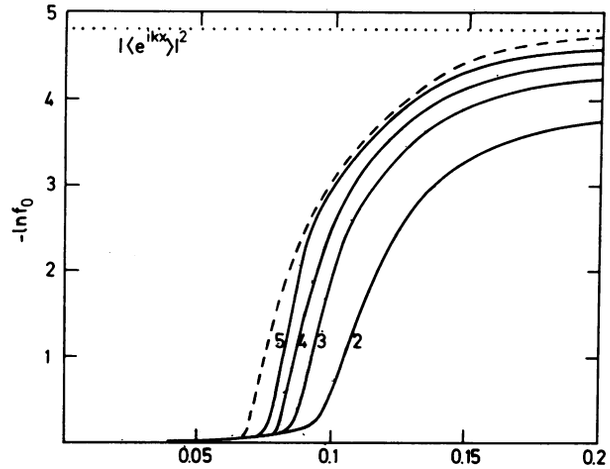

FIG. 2. Lamb–Mössbauer factors determined from a two-Lorentzian representation reproducing μ_0 to μ_{-3}. Solid lines result from the complete potential (Eq. **13**) in the square well $0 \leq x \leq 2x_0$ [x_0 = 1.5 Å, $D = 10^8$ (k_BT/b) Å$^2\cdot$s^{-1}]; the density of substates per Å is indicated. The dashed line results from a coarse-grained description (see text) with $D = \bar{D}\cdot\exp(-E/k_BT)$ ($\bar{D} = 1.513 \times 10^6$ Å$^2\cdot$s^{-1}, $E = 0.632\cdot b$); these constants were obtained from a numerical fit to Eq. **20**. The dotted line represents the Debye–Waller factor for the square well.

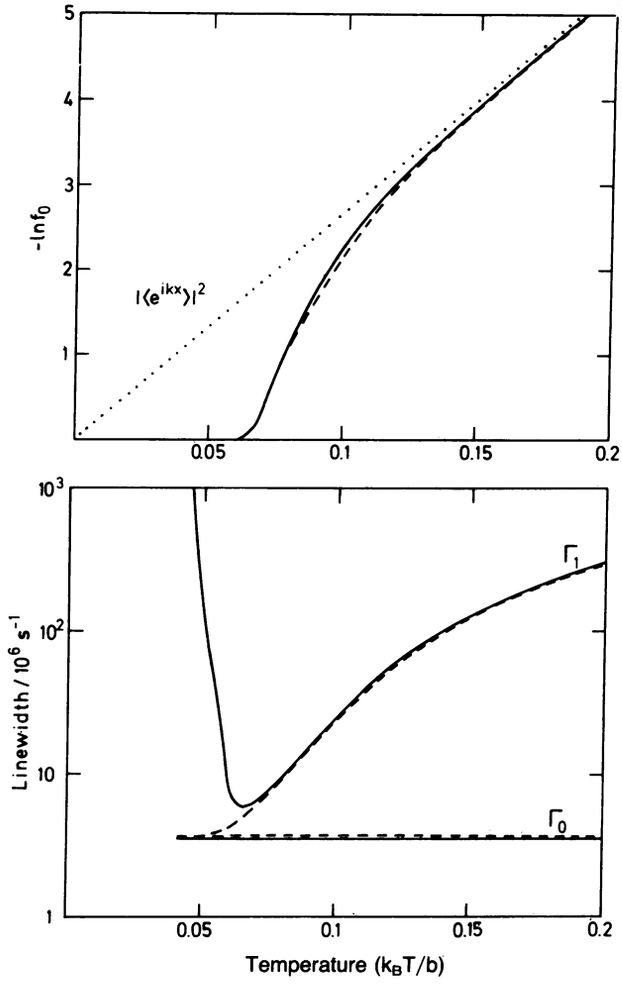

FIG. 3. Lamb–Mössbauer factor (*Upper*) and linewidths (*Lower*) determined from a two-Lorentzian representation reproducing μ_0 to μ_{-3} for a ^{57}Fe Brownian atom moving in a harmonic envelope potential $U(x) = b(x/x_0)^2$ with the potential (Eq. **13**) superimposed (x_0 = 1 Å, n = 6). The solid line results from the complete potential and D as in Fig. 2. The dashed line results from the coarse-grained description, $\bar{D}$ and E as in Fig. 2. The dotted line (*Upper*) represents the Debye–Waller factor $|\langle\exp(ikx)\rangle|^2$ of the harmonic envelope potential.

coarse-grained description of diffusion in a harmonic envelope potential accounting for conformational substates by a diffusion coefficient with Arrhenius-type temperature dependence $D = \bar{D}\cdot\exp(-E/k_BT)$. In order to account accurately for the data, it has proven necessary to introduce at least one additional substate ss^* with the following dynamical property: the rate constants to and from ss^* are chosen such that the equilibrium probability to be in the substate is given by

$$p_{ss^*} = l_{ss^*}\exp(\Delta G/k_BT)/[l_h + l_{ss^*}\exp(\Delta G/k_BT)], \quad [21]$$

where $l_h = (\langle x^2\rangle)^{1/2}$ is the mean width of the distribution in the harmonic envelope potential and is in the range 0.2–0.3 Å within the temperature range considered; $l_{ss^*} << k^{-1}$ is the width of the substate, and $\Delta G = \Delta E - \Delta S\cdot T$ denotes the free energy change connected with the transition from substate to envelope potential. In our calculation the diffusion space is "discretized," and ss^* is represented by a single point at the envelope potential minimum; rate constants to and from ss^* are D/δ^2 and $(D/\delta^2)\cdot\exp(-\Delta G/k_BT)$, respectively, where δ is the discretization length. From a comparison of predictions and data, we obtained E = 0.16 eV; for the entropy

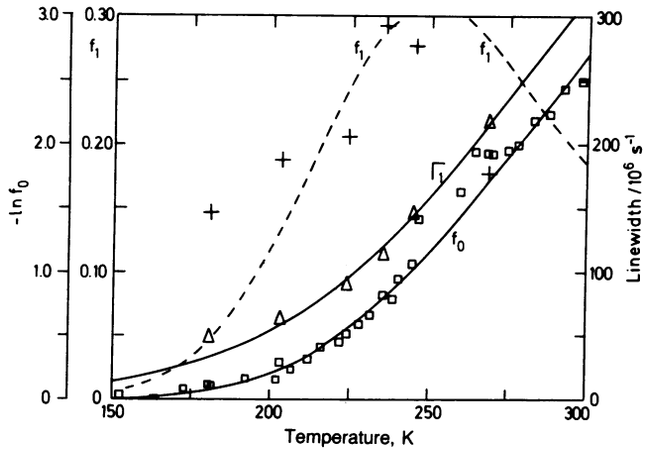

FIG. 4. Comparison of predicted and observed (5, 16) Mössbauer line shapes at different temperatures. f_0 denotes the Lamb–Mössbauer factor (□, —); f_1 denotes the amplitude (+, ---) and Γ_1 the width (△, —) of the broad line. As done in ref. 16, we subtracted the amplitude for a superimposed harmonic mode. The curves result from a three-Lorentzian representation of the spectrum, reproducing μ_0 to μ_{-5} for a ^{57}Fe Brownian atom in a harmonic potential $U(x) = (1/2)(x/x_0)^2$ and an additional substate at the potential minimum (see text) with $\Delta E/k_B = 1900$ K and $l_{ss^*}\exp(-\Delta S/k_B) = 1.61 \times 10^{-4}$ Å. The shape of the harmonic potential has been chosen in accordance with the high temperature x-ray data for $\langle x^2 \rangle$ in ref. 1 by setting $k_B x_0^2 = 3.6 \times 10^{-4}$ Å^2/K. The diffusion coefficient assumed is $D = \bar{D}\cdot\exp(-E/k_BT)$ with $\bar{D} = 8.25 \times 10^8$ Å^2/s and $E/k_B = 1100$ K. The third line in the theoretical spectrum was assumed to represent the background and has been omitted.

contribution we found $l_{ss^*}\exp(-\Delta S/k_BT) = 1.61 \times 10^{-4}$ Å. This value, in comparison with l_h, implies that ss^* assumes only a very small volume of phase space. This implication has been suggested previously in refs. 16 and 22. The small phase space volume of ss^* may contribute to the observed flexibility of proteins, since the protein, once it has fluctuated out of the narrow substate ss^*, needs a long time to find and fall back into this substate.

The small magnitude of the phase space volume of ss^* can be readily understood if one considers the fact that the stochastic motion of ^{57}Fe coupled to the many degrees of freedom of the protein is taking place in a space of high dimension N. The ratio r of the extension of ss^* to the extension of the thermal motion in any coordinate is certainly smaller than one; the ratio of the volume of ss^* to the volume of thermal motion is r^N—i.e., must be a small number for large N. This feature of the substates may pose problems for the determination of stable protein conformations by computer simulation.

Fig. 4 demonstrates that the resulting predictions agree well with the observations. Inaccuracies are found only for the amplitude f_1 of the broadened line. The decrease of the amplitude f_1 at higher temperatures results from a shift of the intensity to very broad lines, considered to represent the background of the Mössbauer spectrum. The differentiation between background and broad lines entails also a certain degree of arbitrariness, which could explain the deviation of predictions and data. The diffusion coefficient fitted to the data has the value $\bar{D} = 8.25 \times 10^8$ Å^2/s, which is in the range of values observed for the diffusion coefficients of lipid probes in the liquid-crystalline phase of lipid membranes (23). The activation energy for the diffusive motion is about 0.09 eV. In order to account for the Debye–Waller factor as observed by x-ray scattering at very low temperatures (i.e., a nonvanishing $\langle x^2 \rangle$ value), one needs to include more than one substate ss^* or one needs to assume randomly positioned ss^* substates in an ensemble of proteins (static disorder).

Outlook

We believe that our method for the evaluation of the structure factor $\sigma(\omega)$ provides a new basis for analyzing Mössbauer spectra of proteins since it allows a model-independent analysis—i.e., for arbitrary (one-dimensional) potentials. We like to mention, however, that a unique, time-invariant potential for the Mössbauer particle as used in this paper may not represent fully the complex dynamics of a protein atom. One may rather consider a distribution of potential shapes (e.g., barrier heights as suggested in refs. 1 and 2) leading to a distribution of Arrhenius-type diffusion coefficients and also study the effect of fluctuating potentials and high-dimensional motions.

The authors thank A. Brünger, E. W. Knapp, F. Parak, and Z. Schulten for helpful discussions. Furthermore we thank E. W. Knapp and F. Parak for supplying us with the original data of refs. 5 and 16 and providing us with a preprint of ref. 22. This work has been supported by the Deutsche Forschungsgemeinschaft (SFB-143C1).

1. Frauenfelder, H., Petsko, G. A. & Tsernoglu, D. (1979) *Nature (London)* **280,** 558–563.
2. Austin, R. H., Beeson, K. W., Eisenstein, L., Frauenfelder, H. & Gunsalus, I. C. (1975) *Biochemistry* **14,** 5355–5373.
3. Keller, H. & Debrunner, P. G. (1980) *Phys. Rev. Lett.* **45,** 68–71.
4. Parak, F., Frolov, E. N., Mössbauer, R. L. & Goldanskii, V. I. (1981) *J. Mol. Biol.* **145,** 825–833.
5. Parak, F., Knapp, E. W. & Kucheida, D. (1982) *J. Mol. Biol.* **161,** 177–194.
6. Hartmann, H., Parak, F., Steigemann, W., Petsko, G. A., Ringe Ponzi, D. & Frauenfelder, H. (1982) *Proc. Natl. Acad. Sci. USA* **79,** 4967–4971.
7. Bauminger, E. R., Cohen, S. G., Nowik, I., Ofer, S. & Yariv, J. (1983) *Proc. Natl. Acad. Sci. USA* **80,** 736–740.
8. Mayo, K. H., Parak, F. & Mössbauer, R. L. (1981) *Phys. Lett. A* **82,** 468–470.
9. Parak, F., Frolov, E. N., Kononenko, A. A., Mössbauer, R. L., Goldanskii, V. I. & Rubin, A. B. (1980) *FEBS Lett.* **117,** 368–372.
10. Cohen, S. G., Bauminger, E. R., Nowik, I. & Ofer, S. (1981) *Phys. Rev. Lett.* **46,** 1244–1247.
11. Haken, H. (1977) *Synergetics* (Springer, Berlin), pp. 152–158.
12. McCammon, J. A., Gelin, B. R. & Karplus, M. (1977) *Nature (London)* **267,** 585–590.
13. Nadler, W. & Schulten, K. (1983) *Phys. Rev. Lett.* **51,** 1712–1715.
14. Szabo, A., Schulten, K. & Schulten, Z. (1980) *J. Chem. Phys.* **72,** 4350–4357.
15. Schulten, K., Schulten, Z. & Szabo, A. (1981) *J. Chem. Phys.* **74,** 4426–4432.
16. Knapp, E. W., Fischer, S. F. & Parak, F. (1982) *J. Phys. Chem.* **86,** 5042–5047.
17. Knapp, E. W., Fischer, S. F. & Parak, F. (1983) *J. Chem. Phys.* **78,** 4701–4711.
18. Németh, G., Ág, A. & Páris, G. (1981) *J. Math. Phys. (NY)* **22,** 1192–1195.
19. Jones, W. B., Thron, W. J. & Waadeland, H. (1980) *Trans. Am. Math. Soc.* **261,** 503–529.
20. Schulten, K., Brünger, A., Nadler, W. & Schulten, Z. (1984) in *Synergetics: From Microscopic to Macroscopic Order*, ed. Frehland, E. (Springer, Berlin), pp. 80–89.
21. Festa, R. & Galleani d'Agliano, E. (1978) *Physica A* **90,** 229–244.
22. Parak, F. & Knapp, E. W. (1984) *Proc. Natl. Acad. Sci. USA* **81,** in press.
23. Vaz, W. L. C., Derzko, Z. I. & Jacobson, K. A. (1982) in *Membrane Reconstitution*, eds. Poste, G. & Nicolson, G. L. (Elsevier Biomedical, Amsterdam), pp. 83–136.